

Semi-Analytical Dynamic Analysis of Spiral-Grooved Mechanical Gas Face Seals

Brad A. Miller

Department of Mechanical and Aerospace
Engineering and Engineering Mechanics,
University of Missouri-Rolla,
1870 Miner Circle,
Rolla, MO 65409-0050

Itzhak Green

George W. Woodruff School of Mechanical
Engineering,
Georgia Institute of Technology,
Atlanta, GA 30332-0405

A novel semi-analytical formulation is presented for the linearized dynamic analysis of spiral-grooved mechanical gas face seals. The linearized rotordynamic properties of the gas film are numerically computed and then represented analytically by a constitutive model consisting of a cosine modified Prony series. The cosine modification enables the Prony series to characterize the gas film properties of face seals in applications with large compressibility numbers. The gas film correspondence principle is then employed to couple the constitutive model to the dynamics of the mechanical face seal. Closed-form solutions are presented for the transient natural response to initial velocity conditions, the steady-state response to rotor runout and initial stator misalignment, the transmissibility ratios, and the stability threshold. Results from the closed-form solutions are all within a few percent of the results from a full nonlinear numerical simulation.

[DOI: 10.1115/1.1510876]

Introduction

Noncontacting mechanical gas face seals (Fig. 1) are used in high speed rotating machinery to obstruct or prevent sealed gas from escaping around a rotating shaft from one compartment to another. Sealing is effected by forcing the leaking gas to escape through a small gap between the stator and rotor mating faces. The gap geometry has a significant effect on the sealing performance; in theory, a smaller gap increases the resistance to escaping flow. The ideal seal design then maximizes this resistance by maintaining the face separation as narrow and as parallel as possible, even when inherent flaws, such as rotor runout and initial stator misalignment, are present. Such misalignments occur in all practical seals because of manufacturing tolerances, assembly imperfections, mechanical warping, face wear, bent shafts, etc.

In general, face seals are designed so that one or both of the seal rings are flexibly mounted to allow active tracking of misalignments. This flexibility adds to the complexity of dynamic interaction between the mating rings generates hydrodynamic pressure in the sealing region, which can be advantageous or detrimental. In a well designed seal, the gas film contributes both stiffness, which actively promotes face separation, and damping, which helps to dissipate energy from shock disturbances. However, these gas film properties, under some circumstances, can also contribute to seal failure by instigating instabilities, and neglecting the gas film contribution can lead to seal designs with poor dynamic performance and sometimes catastrophic results. Therefore, a critically important challenge is to develop dynamic analysis tools for the design of mechanical face seals that incorporate the complex properties of the gas film.

To date, the dynamic analysis of gas face seals has relied mostly on the direct numerical simulation of motion [1–6]. Direct numerical simulations are useful because they are faster and less expensive than prototype development or experimental investigations and because they can include the nonlinear effects. Though they yield a significant amount of detailed information about the overall seal motion, numerical simulations are computationally intensive and not insightful into the influence of any one compo-

nent on the seal motion. Therefore, direct numerical simulations are not conducive to parametric studies of modifications to the geometry or operating conditions, which are often involved in seal design. On the other hand, small perturbation techniques and linear analytical methods are more practical and cost efficient alternatives. Analytical dynamic analysis methods are available for liquid lubricated mechanical face seals [7], but the same techniques are not applicable to gas face seals because of gas compressibility effects. So far, two specific obstacles have hindered the development of analytical techniques for gas face seals: (i) closed-form representations of the gas film stiffness and damp-

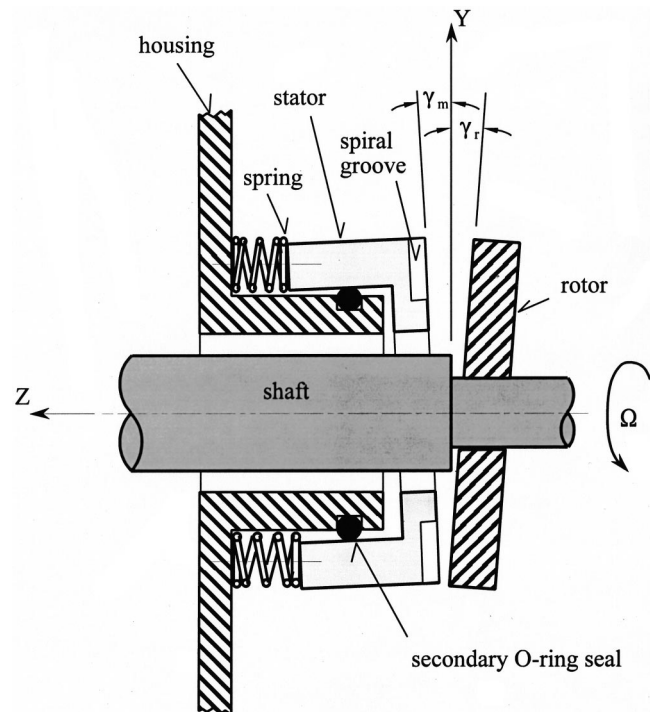


Fig. 1 Schematic of a mechanical face seal in a flexibly mounted stator configuration

Contributed by the Tribology Division of THE AMERICAN SOCIETY OF MECHANICAL ENGINEERS for presentation at the ASME/STLE Tribology Conference, Cancun, Mexico October 27–30, 2002. Manuscript received by the Tribology Division April 16, 2002; revised manuscript received July 25, 2002. Associated Editor: J. A. Tichy.

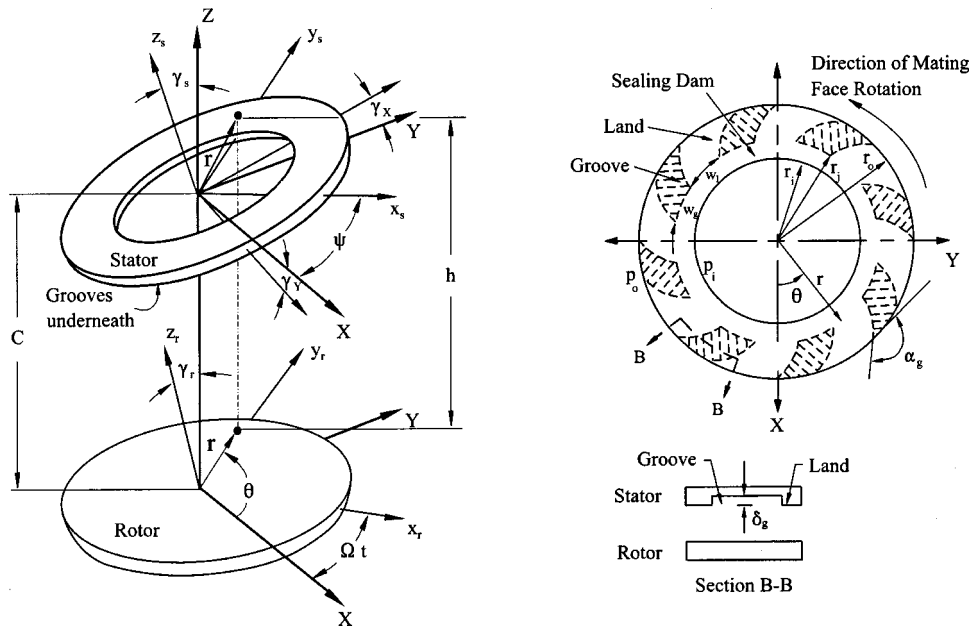


Fig. 2 Mechanical face seal kinematic model and spiral groove geometry profile

ing properties have not been developed and (ii) a method for coupling the gas film properties to the other elements in the system is not available.

The objective of this paper is to breach this apparent gap and present a semi-analytical dynamic analysis technique for mechanical gas face seals. The new technique is comprised of three steps. In the first step, the linearized gas film properties are characterized using a conventional numerical technique. Three such techniques have been presented in literature: the small perturbation method [8–10], the step jump method [14], and the direct numerical frequency response method [11]. It is important to note that in this entire analysis process, this first step (i.e., computing the gas film stiffness and damping properties) is the only part that necessarily requires numerical computations by computer. In the second step, an analytical constitutive model is constructed that accurately represents the gas film rotordynamic properties in closed-form. Then finally, the constitutive model is coupled to the equations of motion using the gas film correspondence principle, allowing for closed-form solutions of the resulting equations. Recently, an analytical solution for the dynamics of gas face seals that replicates [13] has been presented by Ruan [10], but the technique does not incorporate the frequency dependence of the gas film properties. The procedure developed here is not constrained by the limitation of constant (frequency independent) gas film properties; instead, these complex properties are totally incorporated using the correspondence principle.

Mechanical Face Seal Dynamic Model

A schematic of the mechanical seal model is shown in Fig. 1. One seal ring (stator) is flexibly mounted to the housing by an elastomeric o-ring, acting as the secondary seal, and a spring. The other seal ring (rotor) is rigidly mounted to the rotating shaft. The stator is flexibly mounted ideally to allow successful tracking of the rotor motion and thereby to minimize the relative misalignment between the two seal rings. Often, spiral grooves are machined into one of the faces to improve sealing and to facilitate face separation during initial startup.

A kinematic model of the mechanical seal is shown in Fig. 2. The stator's flexible mounting admits three degrees of freedom, including tilts about the inertial X and Y axes (γ_X and γ_Y , respectively) and axial translation of the stator center (Z), measured from its equilibrium position, C_0 . A rotating reference frame,

x_s, y_s, z_s , is used to describe the stator orientation. The x_s, y_s plane is chosen to lie coincident with the stator face; however, the frame rotates to keep the x_s axis perpendicular to Z . Precession of axis x_s about Z is measured by the angle ψ from the X axis, and the nutation angle, γ_s , gives the stator tilt with respect to Z . A similar reference frame, x_r, y_r, z_r , is defined for the rotor so that γ_r measures the rotor tilt (runout) with respect to Z . The tilt, γ_r , takes place about the X_r axis, which precesses at a constant rate of Ω . Figure 1 shows the rotor runout at the particular instant when the x_r axis is pointing into the page.

The stator and rotor tilt angles are small, on the order of one milliradian or smaller, so the tilts can be treated as vectors. In this case, the stator tilt vector ($\vec{\gamma}_s$) and the rotor tilt vector ($\vec{\gamma}_r$) can be decomposed into components along the inertial X and Y axes,

$$\vec{\gamma}_s = \gamma_X \vec{e}_X + \gamma_Y \vec{e}_Y,$$

$$\vec{\gamma}_r = \gamma_r \cos(\Omega t) \vec{e}_X + \gamma_r \sin(\Omega t) \vec{e}_Y. \quad (1)$$

where \vec{e}_X and \vec{e}_Y are unit vectors in the X and Y directions, respectively. In this formulation, $\vec{\gamma}_r$ is initially aligned with the inertial X axis. During operation, the relative misalignment between the stator and rotor is one of the critical factors that influences sealing performance. For example, a large relative misalignment amplitude or phase difference is deleterious, causing excessive leakage and/or seal face contact. The relative misalignment, $\vec{\gamma}_{rel}$, is the vector subtraction of the stator and rotor tilts,

$$\vec{\gamma}_{rel} = \vec{\gamma}_s - \vec{\gamma}_r = \{\gamma_X - \gamma_r \cos(\Omega t)\} \vec{e}_X + \{\gamma_Y - \gamma_r \sin(\Omega t)\} \vec{e}_Y. \quad (2)$$

The relative misalignment vector reveals both the difference in magnitude and phase between the stator and rotor, making it an excellent indicator of the stator tracking ability and overall sealing performance. Ideally, the relative misalignment is minimized for minimal leakage.

The seal studied in this work contains spiral grooves manufactured on the face of the stator, as depicted in Fig. 2. A total of N_g spiral grooves are present at a depth of δ_g . The land width to groove width fraction, measured by β , and the equation for the groove curvature are defined as

$$\beta = \frac{w_g}{w_g + w_l}; \quad r = r_j e^{\theta \tan(\alpha_g)}, \quad 0 < \alpha_g < 180 \text{ deg}, \quad (3)$$

where α_g is the spiral angle and $\alpha_g = 90$ deg corresponds to radial grooves. The radius, r_j , marks the junction between the spiral groove region and the sealing dam region.

The applied forces and moments on the stator come from the flexible support and the gas film pressure. For this analysis, the flexible support is assumed to have a constant axial stiffness and damping of k_{sZ} and d_{sZ} , respectively. According to Green and Etsion [7], the flexible support also contributes angular stiffness and damping of

$$k_{s\gamma} = \frac{1}{2} k_{sZ} \cdot r_o^2, \quad d_{s\gamma} = \frac{1}{2} d_{sZ} \cdot r_o^2, \quad (4)$$

assuming that the support forces act at the outer radius, r_o .

During operation, the relative motion between the seal rings and the pressure difference across the inner and outer seal radii generate hydrodynamic and hydrostatic pressure between the seal faces. Assuming the gas flow is ideal, isothermal and inertialess, the pressure distribution in the gas film is obtained from the compressible form of the Reynolds equation [12],

$$\vec{\nabla} \cdot [p h^3 \vec{\nabla} p - 6 \mu \Omega r p h \vec{e}_\theta] = 12 \mu \frac{\partial(p h)}{\partial t}. \quad (5)$$

The polar coordinate gradient operator is presumed here, and the following boundary conditions apply:

$$\begin{aligned} p(r_i, \theta, t) &= p_i, \\ p(r_o, \theta, t) &= p_o, \\ p(r, 0, t) &= p(r, 2\pi, t). \end{aligned} \quad (6)$$

Solution of the Reynolds equation subject to the boundary conditions yields the pressure, from which the gas film force and moments, F_Z , M_X , and M_Y , are found by appropriately integrating the pressure over the sealing area. The gas film force and moments and the seal ring motion are coupled by the film thickness, h , and the squeeze term, $\partial h / \partial t$, through the stator degrees of freedom,

$$\begin{aligned} h(r, \theta) &= C_0 + Z + r \gamma_X \sin(\theta) - r \gamma_Y \cos(\theta) + \langle \delta_g \rangle \\ &\quad - \gamma_r r \sin(\theta - \Omega t), \\ \frac{\partial h(r, \theta)}{\partial t} &= \dot{Z} + r \dot{\gamma}_X \sin(\theta) - r \dot{\gamma}_Y \cos(\theta) + \Omega \gamma_r r \cos(\theta - \Omega t). \end{aligned} \quad (7)$$

The $\langle \delta_g \rangle$ term is only added inside a groove and creates discontinuity in h but not in $\partial h / \partial t$.

The dynamic motion of the stator is governed by the equations of motion [7],

$$\begin{aligned} m \ddot{Z} &= -F_{Z,eq} + F_Z - k_{sZ} Z - d_{sZ} \dot{Z}, \\ I \ddot{\gamma}_X &= M_X - k_{s\gamma} \gamma_X - d_{s\gamma} \dot{\gamma}_X + M_{Xi}, \\ I \ddot{\gamma}_Y &= M_Y - k_{s\gamma} \gamma_Y - d_{s\gamma} \dot{\gamma}_Y. \end{aligned} \quad (8)$$

The force, $F_{Z,eq}$, which results from static deflection in the support and external back pressure, offsets the gas film force at equilibrium to establish the reference axial position of the stator, C_0 . For the situations studied here, the target, or ideal, equilibrium state is when the stator is initially aligned with the rotor. Under these conditions, the gas pressure at equilibrium provides no moment. In Eq. (8), the moment M_{Xi} accounts for the initial stator misalignment, γ_m , caused by manufacturing tolerances and inevitable imperfections in the seal assembly process. Without loss of generality, the misalignment is arbitrarily assumed to occur about

the X axis. Using the model introduced by [7], the magnitude of the moment produced by the initial stator tilt is given by

$$M_{Xi} = k_{s\gamma} \gamma_m, \quad (9)$$

where $k_{s\gamma}$ is the angular stiffness of the flexible support.

A full dynamic analysis of the seal system requires simultaneous solution of the kinetic and lubrication equations. Current dynamic analysis techniques focus mainly on direct numerical simulations of motion, but analytical techniques are superior for design purposes because the solutions are available in closed-form. Before an analytical solution technique can be employed, the gas film properties must first be available in analytical format.

Analytical Characterization of Gas Film Rotordynamic Properties

The gas film stiffness, $S_{ij}(\omega)$, and damping, $D_{ij}(\omega)$, characterize the linear reaction of the gas film force and moments to small sinusoidal stator displacements about equilibrium and to the corresponding velocity, respectively. The ω argument indicates the excitation-frequency dependence of these properties. Since the seal model has three degrees of freedom, there are a total of nine terms for both of these quantities with the i subscript corresponding to the generalized force (F_Z , M_X , or M_Y), and the j subscript corresponding to the generalized displacement (Z , γ_X , or γ_Y). The stiffness and damping together make up the complex-valued gas film frequency response, $G_{ij}(\omega)$, where

$$G_{i,j}(\omega) = S_{i,j}(\omega) + j \omega D_{i,j}(\omega). \quad (10)$$

The real part of the frequency response is also called the storage modulus, and the imaginary part is called the loss modulus.

The gas film properties can also be characterized in the time domain by a series of step responses. The step response is a measure of the transient gas film generalized force response to a small step jump in one degree of freedom. In this context, the step response physically represents the transient gas film stiffness. Under the assumption that the force response is linear, which is valid if the relative motion remains small about equilibrium, the step response is related to the frequency response by the following integral transformation [13],

$$G_{i,j}(\omega) \equiv k_{i,j}(0) + \int_0^\infty \dot{k}_{i,j}(\tau) e^{-j\omega\tau} d\tau. \quad (11)$$

The right hand side of this equation can be simplified to yield

$$G_{i,j}(\omega) \equiv j \omega K_{i,j}(\omega). \quad (12)$$

Here $K(\omega)$ is the Fourier transform of $k(t)$. In the Laplace domain, the relationship is

$$G_{i,j}(s) \equiv s K_{i,j}(s), \quad (13)$$

where $K(s)$ is the Laplace transform of $k(t)$.

The rotordynamic properties are computed with respect to the equilibrium state of perfect seal ring alignment. Symmetry and other conditions dictate that only three of the nine terms are unique; therefore, the step response and frequency response terms can be assembled into the following reduced matrices [11],

$$\begin{aligned} \underline{k}(t) &= \begin{bmatrix} k_{F_Z, Z} & 0 & 0 \\ 0 & k_{M_X, \gamma_X} & -k_{M_Y, \gamma_X} \\ 0 & k_{M_Y, \gamma_X} & k_{M_X, \gamma_X} \end{bmatrix}, \\ \underline{G}(\omega) &= \begin{bmatrix} G_{F_Z, Z} & 0 & 0 \\ 0 & G_{M_X, \gamma_X} & -G_{M_Y, \gamma_X} \\ 0 & G_{M_Y, \gamma_X} & G_{M_X, \gamma_X} \end{bmatrix}. \end{aligned} \quad (14)$$

From the formats of these matrices, the axial displacement of the stator is clearly decoupled from the two stator tilts when only the linearized gas film effects are considered.

For any practical seal configuration, direct analytical solutions of the Reynolds equation are not possible, and the rotordynamic properties must be computed by numerical methods. Miller and Green [11] compute the gas film frequency responses and the step responses for all three modes of motion using procedures based on numerical solutions of the full unsteady, nonlinear Reynolds equation. These techniques are employed in this work to characterize the gas film properties.

Any numerical technique yields the gas film properties in numerical form. To formulate a closed-form, analytical representation, the gas film properties are represented by curve fitting an analytical expression to the numerical frequency response or step response data. This process generates an array of functions that form a constitutive model for the gas film. Originally, Elrod et al. [14] used a series of Laguerre polynomials as the base function for the constitutive model, but Laguerre polynomial functions must be used with caution because they can misrepresent the gas film properties and can introduce false instabilities into the dynamic analysis [15]. Alternatively, Miller and Green [13] introduced a simple Prony series (a series of decaying exponential terms) as a base function for the constitutive model, and they showed that it does not suffer from the same deficiencies as Laguerre polynomials. They successfully used the Prony series to fit data for gas slider bearings and showed that it worked adequately for conditions of low or moderate compressibility numbers. However, at large compressibility numbers, the Prony series alone is incapable of sufficiently capturing all the relevant properties. At high speeds, the step response curves display small, damped oscillatory features. Since the Prony series is a monotonically increasing or decreasing time domain function, it cannot reproduce this behavior. However, the Prony series can be modified to overcome this shortcoming by adding a cosine product to each exponential term in the series,

$$k_{i,j}(t) = k_{i,j}(\infty) + \sum_{n=1}^N A_{i,j,n} \cdot \cos(v_{i,j,n}t + \phi_{i,j,n}) \cdot e^{-\alpha_{i,j,n}t}. \quad (15)$$

The term, $k_{i,j}(\infty)$, is the asymptotic value of the step response.

Applying a Laplace transform to the modified Prony series and multiplying by s yields

$$sK_{i,j}(s) = k_{i,j}(\infty) + \sum_{n=1}^N A_{i,j,n} \cdot s \cdot \frac{(s + \alpha_{i,j,n})\cos(\phi_{i,j,n}) - v_{i,j,n}\sin(\phi_{i,j,n})}{(s + \alpha_{i,j,n})^2 + v_{i,j,n}^2}. \quad (16)$$

It is important for the constitutive model to be representable in the Laplace domain since the gas film correspondence principle couples the gas film properties to the other seal elements in the Laplace domain. Furthermore, the corresponding frequency domain relationship is found simply by replacing s with $j\omega$ in Eq. (16).

As an example of computing the constitutive model, consider the mechanical seal detailed in Table 1. Three particular operating conditions are considered. The gas film properties for each case have previously been numerically computed by Miller and Green [11]. The non-zero step responses and frequency responses are shown in Figs. 3 and 4, respectively. The curves from the corresponding constitutive models are also shown as dashed lines in the figures, and the excellent agreement is evident. Table 2 lists the constitutive model parameters where the number of terms in each series was chosen by a trial and error procedure. The values for the parameters, $A_{i,j,n}$, $\alpha_{i,j,n}$, $v_{i,j,n}$, and $\phi_{i,j,n}$, were determined using a curve fitting process on the complex frequency responses. Although it is also possible to use the step responses, in most

Table 1 Mechanical face seal parameters

Outer Radius, r_o	60.0 mm
Dam Radius, r_j	51.6 mm
Inner Radius, r_i	48.0 mm
Stead-State Clearance, C_0	6.0 μm
Angular Velocity, Ω	<i>varies</i>
Gas Viscosity, μ	$1.8 (10)^{-5} \text{ N}\cdot\text{s}/\text{m}^2$
Pressure at Inner Radius, P_i	0.2 MPa
Pressure at Outer Radius, P_o	0.1 MPa
Stator Mass, m	1.0 kg
Transverse Moment of Inertia, I	$1.8 (10)^{-3} \text{ kg}\cdot\text{m}^2$
Number of Grooves, N_g	12
Spiral Groove Angle, α	160 deg
Land to Groove Width Ratio, β	0.5
Groove Depth, δ_g (μm)	12.0 μm
Support Axial Stiffness, k_{sz}	$5.0 (10)^5 \text{ N}/\text{m}$
Support Axial Damping, d_{sz}	300.0 $\text{N}\cdot\text{s}/\text{m}$
Support Angular Stiffness, $k_{s\gamma}$	900.0 $\text{N}\cdot\text{m}/\text{rad}$
Support Angular Damping, $d_{s\gamma}$	0.54 $\text{N}\cdot\text{m}\cdot\text{s}/\text{rad}$

instances the curve fit using the frequency responses gives a preferable fit since the dynamic characteristics of the gas film are better portrayed in the frequency domain than in the time domain. In most cases, a small number of terms provides an adequate fit.

The Gas Film Correspondence Principle: Coupling the Gas Film to the Seal Elements

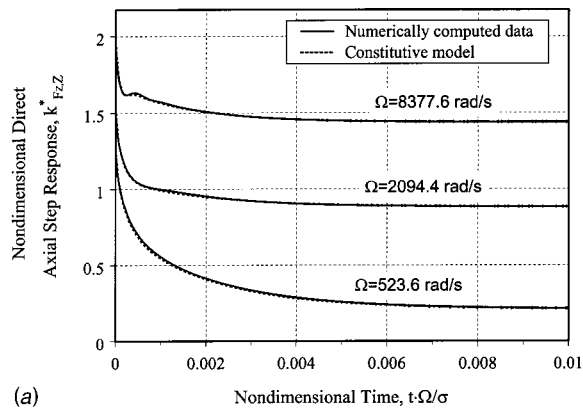
Once the gas film constitutive model has been developed, the next step is to integrate the gas film properties into the seal dynamic model using the gas film correspondence principle. The correspondence principle follows directly from the linearized gas film constitutive law [13],

$$f_i(t) - f_{i,eq} = - \sum_{j=1}^3 \left[k_{i,j}(0)x_j(t) + \int_0^t \dot{k}_{i,j}(\tau)x_j(t - \tau) d\tau \right], \quad (17)$$

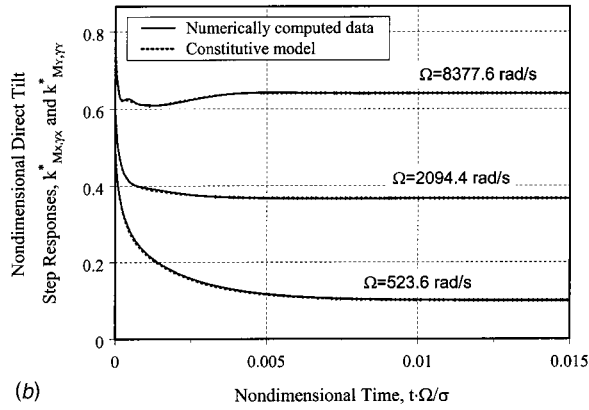
which expresses the generalized gas film forces ($f_i = F_Z$, M_X , or M_Y) as a sum of convolution integrals containing the corresponding step responses and generalized displacement variables ($x_j = Z$, γ_X , or γ_Y). The term $f_{i,eq}$ represents the equilibrium value of the generalized gas film force. The constitutive law is formulated on the basis that the gas film force and moments behave linearly in response to small step displacements of the seal ring. In this formulation, the effects from motion in each degree of freedom are considered separately and superposed to yield the net force effect. The Laplace transform of Eq. (17) yields the Laplace domain representation,

$$F_i(s) - f_{i,eq} = - \sum_{j=1}^3 sK_{i,j}(s)X_j(s). \quad (18)$$

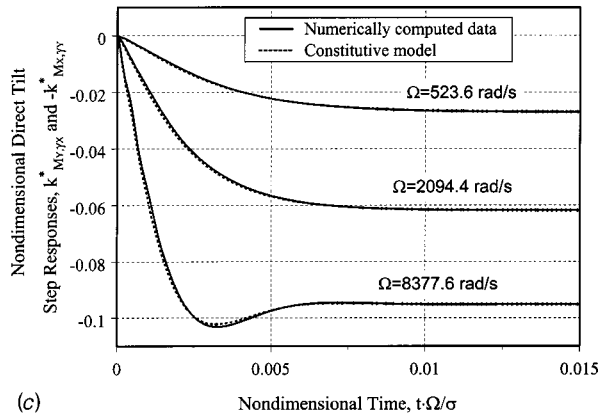
The gas film correspondence principle is applied in the following manner. First, the generalized gas film forces are modeled using a set of pseudo linear springs to represent the net gas film



(a)



(b)

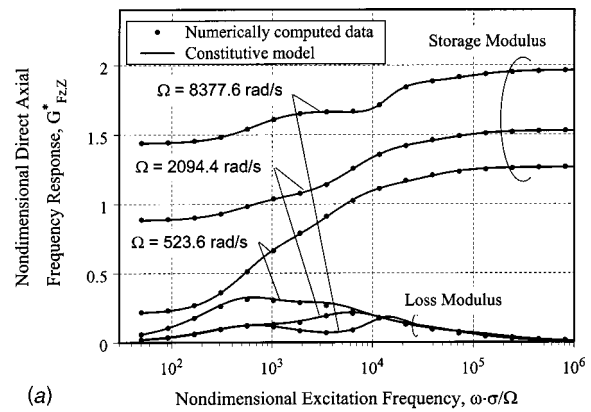


(c)

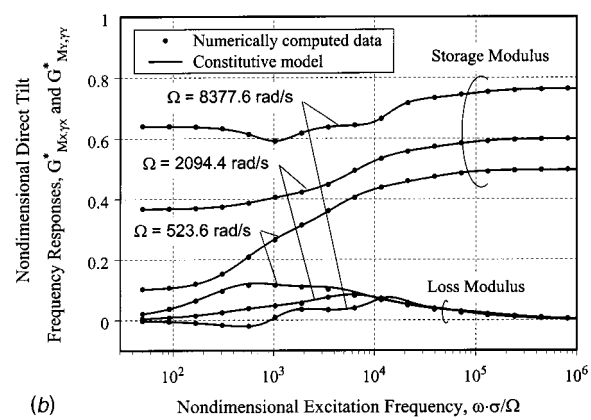
Fig. 3 Step responses computed by numerical solution and the approximate constitutive model; (a) Direct axial step responses; (b) Direct tilt step responses; and (c) Cross-coupled tilt step responses.

stiffness. The wobbling motion of the rotor due to runout harmonically oscillates the film thickness, providing a time varying moment on the stator acting through the gas film stiffness. The gas film force and moments are proportional to the relative position between the stator and rotor. Then according to Eq. (2), the net gas film force and moments on the stator are

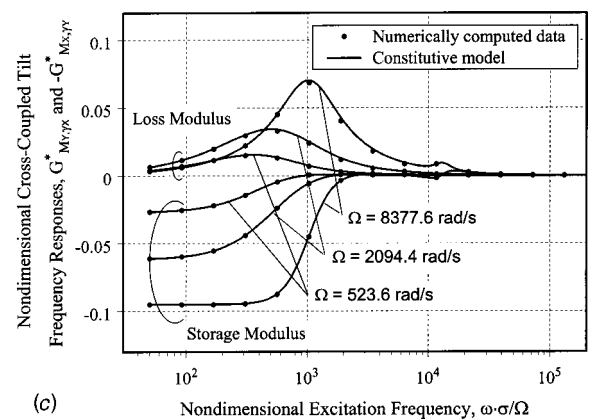
$$\begin{cases} F_Z(t) - F_{eq} \\ M_X(t) \\ M_Y(t) \end{cases} = \begin{bmatrix} -k_{F_Z, Z, g} & 0 & 0 \\ 0 & -k_{M_X, \gamma_X, g} & k_{M_Y, \gamma_X, g} \\ 0 & -k_{M_Y, \gamma_X, g} & -k_{M_X, \gamma_X, g} \end{bmatrix} \times \begin{cases} Z(t) \\ \gamma_X(t) - \gamma_r \cos(\Omega t) \\ \gamma_Y(t) - \gamma_r \sin(\Omega t) \end{cases} \quad (19)$$



(a)



(b)



(c)

Fig. 4 Frequency responses computed by numerical solution and the approximate constitutive model; (a) Direct axial frequency responses; (b) Direct tilt frequency responses; and (c) Cross-coupled tilt frequency responses.

The subscript “g” denotes the pseudo linear spring constants. Next, Eq. (19) is substituted into the equations of motion, Eq. (8), and the Laplace transform is performed on the resulting equations. Then, according to the correspondence principle, the complex nature of the gas film properties is incorporated simply by substituting the appropriate $sK_{i,j}(s)$ for the corresponding pseudo spring modulus, $k_{i,j,g}$. Performing these steps and rearranging yields the following equation for the axial mode,

$$\begin{aligned} \{ms^2 + sK_{F_Z, Z}(s) + k_{sZ} + sd_{sZ}\}Z(s) \\ = m\{sZ(0) - \dot{Z}(0)\} + d_{sZ}Z(0). \end{aligned} \quad (20)$$

Table 2 Coefficients in the modified Prony series constitutive model for mechanical face seal

Ω (rad/s)		n	A_n	α_n	ν_n	ϕ_n	$k(\infty)$
8377.6	$k_{F_z, z}$	1	0.247	651	0	-0.25	1.439
		2	0.211	8266	9901	0.33	
		3	0.0868	89923	0	-0.07	
	k_{M_x, γ_x} k_{M_y, γ_y}	1	-0.106	754	760	-1.66	0.640
		2	0.0841	8267	9841	0.31	
		3	0.0331	89166	0	-0.01	
	k_{M_y, γ_x} $-k_{M_x, \gamma_y}$	1	-0.0962	713	764	3.07	-0.0951
		2	0.00234	2559	12691	.017	
		3	-0.00307	20291	0	0.0	
2094.4	$k_{F_z, z}$	1	0.177	497	0	0.0	0.882
		2	0.387	6293	0	0.0	
		3	0.0844	66418	0	0.0	
	k_{M_x, γ_x} k_{M_y, γ_y}	1	0.0494	700	0	0.0	0.367
		2	0.150	6202	0	0.0	
		3	0.0320	65371	0	0.0	
	k_{M_y, γ_x} $-k_{M_x, \gamma_y}$	1	0.0814	562	0	0.0	-0.0618
		2	-0.0192	1405	0	0.0	
		3	-0.000443	33392	0	0.0	
523.6	$k_{F_z, z}$	1	0.540	509	0	0.0	0.211
		2	0.396	4083	0	0.0	
		3	0.119	37965	0	0.0	
	k_{M_x, γ_x} k_{M_y, γ_y}	1	0.199	522	0	0.0	0.100
		2	0.152	4031	0	0.0	
		3	0.0455	36834	0	0.0	
	k_{M_y, γ_x} $-k_{M_x, \gamma_y}$	1	0.0439	438	0	0.0	-0.0270
		2	-0.0169	871	0	0.0	
		3	-	-	-	-	

Clearly, the axial mode is decoupled from the two angular modes; therefore, the solutions can be treated separately. The solution of Eq. (20) is found by algebraic manipulation to be

$$Z(s) = \frac{m\{sZ(0) - \dot{Z}(0)\} + d_{sz}Z(0)}{ms^2 + sK_{F_z, z}(s) + k_{sz} + sd_{sz}} \quad (21)$$

The characteristic equation for the axial mode is

$$ms^2 + sK_{F_z, z}(s) + k_{sz} + sd_{sz} = 0 \quad (22)$$

Now for the angular modes, the following equations are found,

$$\begin{bmatrix} a_{11} & a_{12} \\ a_{21} & a_{22} \end{bmatrix} \begin{Bmatrix} \Gamma_X(s) \\ \Gamma_Y(s) \end{Bmatrix} = \begin{Bmatrix} b_1 \\ b_2 \end{Bmatrix}, \quad (23)$$

where the matrix coefficients are defined as

$$\begin{aligned} a_{11} &= Is^2 + sK_{M_x, \gamma_x}(s) + k_{s\gamma} + sd_{s\gamma}, \\ a_{12} &= sK_{M_x, \gamma_y}(s), \\ a_{21} &= sK_{M_y, \gamma_x}(s), \\ a_{22} &= Is^2 + sK_{M_y, \gamma_y}(s) + k_{s\gamma} + sd_{s\gamma}, \end{aligned} \quad (24)$$

and where

$$\begin{aligned} b_1 &= I\{s\gamma_X(0) + \dot{\gamma}_X(0)\} + d_{s\gamma}\gamma_X(0) + \gamma_r sK_{M_x, \gamma_x}(s) \frac{s}{s^2 + \Omega^2} \\ &\quad + \gamma_r sK_{M_x, \gamma_y}(s) \frac{\Omega}{s^2 + \Omega^2} + \frac{1}{s}M_{X_i}, \end{aligned}$$

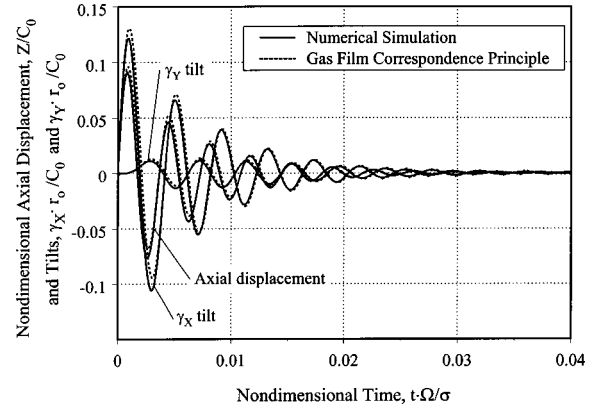


Fig. 5 Stator axial and tilt responses to initial velocity conditions computed by numerical simulation and the gas film correspondence principle ($\Omega = 2094.4$ rad/s)

$$\begin{aligned} b_2 &= I\{s\gamma_Y(0) + \dot{\gamma}_Y(0)\} + d_{s\gamma}\gamma_Y(0) + \gamma_r sK_{M_y, \gamma_x}(s) \frac{s}{s^2 + \Omega^2} \\ &\quad + \gamma_r sK_{M_y, \gamma_y}(s) \frac{\Omega}{s^2 + \Omega^2}. \end{aligned} \quad (25)$$

The general solution for the tilt motion is found to be

$$\Gamma_X(s) = \frac{a_{22}b_1 - a_{12}b_2}{a_{11}a_{22} - a_{12}a_{21}}; \quad \Gamma_Y(s) = \frac{-a_{21}b_1 + a_{11}b_2}{a_{11}a_{22} - a_{12}a_{21}} \quad (26)$$

Also, the characteristic equation for the tilt modes is the determinant of the matrix in Eq. (23),

$$a_{11}a_{22} - a_{12}a_{21} = 0 \quad (27)$$

Furthermore, by exploiting the symmetry of the support and gas film properties, the characteristic equation can be simplified to

$$[Is^2 + sK_{M_x, \gamma_x}(s) + k_{s\gamma} + sd_{s\gamma}]^2 + [sK_{M_y, \gamma_x}(s)]^2 = 0 \quad (28)$$

The characteristic equations given by Eqs. (22) and (28) are valid for all seals with this kinematic model and are useful for studying their stability. Stability analysis will be discussed later.

Several types of analytical solutions are now possible, including expressions for the initial transient response to nonzero initial conditions, the steady-state response to rotor runout and stator misalignment, and stability. Since the equations of motion are linear, the effects from the initial conditions, rotor runout and static stator misalignment can be treated, and solved separately and the total response is then found by the principle of superposition. The novel aspect of this analysis is that the solutions are available in closed-form once the gas film properties have been characterized and the constitutive model formulated. Examples of these solutions will now be presented for the seal detailed in Table 1 with a shaft rotation speed of $\Omega = 2094.4$ rad/s. Where direct numerical simulations are presented, the technique outlined in Miller and Green [4] has been employed.

Simulation of the Natural Transient Response

For simulating the natural transient response to initial conditions, the rotor runout and stator misalignment are set equal to zero so that only the response to nonzero initial velocity conditions is considered. These conditions simulate the response of the system to a shock excitation. In this case, the initial shock imparts an instantaneous linear velocity along the shaft axis of $\dot{Z}(0) = 2$ mm/s and an angular tilt velocity about the X axis of $\dot{\gamma}_X(0) = 0.05$ rad/s. The stator transient response is computed by inverse Laplace transformations of Eqs. (21) and (26), which are performed symbolically using commercial software. Figure 5 shows

comparisons of the analytical solutions with responses computed by a nonlinear direct numerical simulation. The natural frequencies of oscillation and the decay rates predicted by the analytical and numerical solutions are in very good agreement. Also, the correspondence principle accurately captures the coupling between the two tilt modes. The quality of these results verifies that the axial mode is effectively decoupled from the tilt modes and that the constitutive model accurately represents the stiffness and damping properties of the gas film for this configuration.

Steady-State Response to Rotor Runout

The amplitude and direction of the rotor misalignment are measured by the vector, $\tilde{\gamma}_r$, which has been defined in Eq. (1). If the runout is large, the stator is generally less capable of tracking the rotor misalignment, leading to large seal ring separation and excessive leakage. Though the transient response may be significant when the seal experiences a shock disturbance, the transients are usually short as long as the seal is stable. Most of the seal life is spent in steady-state tracking motion; therefore, the steady-state response is used as the preferred indicator of tracking ability. Since the system is linear, the responses caused by the rotor runout and initial stator misalignment can be computed separately and then added later using the principle of superposition. Therefore, neglecting the initial conditions and M_{xi} , the only forcing functions remaining on the right hand side of Eq. (23) (defined as b_1 and b_2 in Eq. (25)) are those terms from the rotor runout. The rotor runout produces a harmonic forcing function at the frequency of shaft rotation, Ω , and the steady-state stator response to this forcing has the same form. Taking advantage of the symmetry of the inertia, support and gas film properties, the stator response can be simplified to

$$\begin{aligned}\gamma_{X,r}(t) &= \gamma_r A \cos(\Omega t - \phi), \\ \gamma_{Y,r}(t) &= \gamma_r A \sin(\Omega t - \phi).\end{aligned}\quad (29)$$

Closed-form expressions for A and ϕ are given by

$$\begin{aligned}A &= \frac{1}{\Delta} \sqrt{(\text{Re}[R_{X,c}] - \text{Im}[R_{Y,c}])^2 + (\text{Re}[R_{X,s}] - \text{Im}[R_{Y,s}])^2}, \\ \tan(\phi) &= \frac{\text{Re}[R_{X,s}] - \text{Im}[R_{Y,s}]}{\text{Re}[R_{X,c}] - \text{Im}[R_{Y,c}]}, \\ \Delta &= a_{11}a_{22} - a_{12}a_{21}.\end{aligned}\quad (30)$$

The terms a_{11} , a_{22} , a_{12} , and a_{21} , are defined in Eq. (24), and $\text{Re}[R]$ and $\text{Im}[R]$ correspond to the real and imaginary parts of R , respectively, where

$$\begin{aligned}R_{X,c}(j\Omega) &= \frac{1}{\Delta} \cdot \{a_{22}j\Omega K_{M_x, \gamma_X}(j\Omega) - a_{12}j\Omega K_{M_y, \gamma_X}(j\Omega)\}, \\ R_{X,s}(j\Omega) &= \frac{1}{\Delta} \cdot \{a_{22}j\Omega K_{M_x, \gamma_Y}(j\Omega) - a_{12}j\Omega K_{M_y, \gamma_Y}(j\Omega)\}, \\ R_{Y,c}(j\Omega) &= \frac{1}{\Delta} \cdot \{-a_{21}j\Omega K_{M_x, \gamma_X}(j\Omega) + a_{11}j\Omega K_{M_y, \gamma_X}(j\Omega)\}, \\ R_{Y,s}(j\Omega) &= \frac{1}{\Delta} \cdot \{-a_{21}j\Omega K_{M_x, \gamma_Y}(j\Omega) - a_{11}j\Omega K_{M_y, \gamma_Y}(j\Omega)\}.\end{aligned}\quad (31)$$

The subscript “r” is added to the tilt vectors in Eq. (29) to indicate that it corresponds to the steady-state response to rotor runout alone. The total stator response is found by vector addition to be

$$\tilde{\gamma}_{s,r} = \{\gamma_r A \cos(\Omega t - \phi)\} \tilde{e}_X + \{\gamma_r A \sin(\Omega t - \phi)\} \tilde{e}_Y, \quad (32)$$

or in complex notation,

$$\tilde{\gamma}_{s,r} = \gamma_r A e^{j(\Omega t - \phi)}. \quad (33)$$

By this analysis, it is clear that the steady-state stator response to rotor runout is proportional to the runout amplitude by the factor

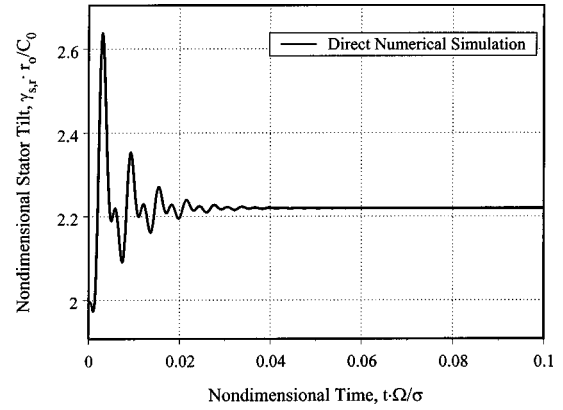


Fig. 6 Stator tilt response to rotor runout alone computed by numerical simulation ($\Omega = 2094.4$ rad/s)

A and lags it by an angle ϕ . For comparison, Fig. 6 shows the numerical simulation of the stator response to a relatively large rotor runout of $\gamma_r \cdot r_o / C_0 = 2.0$. After initial transients have decayed, the seal obviously reaches a steady-state motion of synchronous tracking, where the response amplitude is constant at $\gamma_{s,r} \cdot r_o / C_0 = 2.22$. Using Eq. (30) with the constitutive model parameters in Table 2, the correspondence principle gives a steady-state value of $\gamma_{s,r} \cdot r_o / C_0 = 2.21$ for the stator response, with a relative difference of approximately 0.5 percent.

This nonlinear simulation required 258 minutes of CPU time on a personal computer with a 450 MHz Pentium® II processor. On the other hand, it required 134 minutes of CPU time on the same computer to numerically compute the gas film properties via the step jump method (see Figs. 3 and 4) and then obtain the constitutive model parameters in Table 2. Note, however, that these gas film properties must be computed only one time. Once the analytical constitutive model is obtained, the closed-form solution contains no more computational overhead, which provides a significant time savings in analysis and design.

Steady-State Response to Initial Stator Misalignment

For the seal response to initial stator misalignment, the initial conditions and rotor runout are ignored. Now since the stator misalignment provides a constant moment proportional to the support stiffness, the stator response will also be constant at steady-state. To find the long-time, constant response at steady-state, Eq. (26) is employed with the final value theorem to give

$$\begin{aligned}\gamma_{X,m} &= \lim_{s \rightarrow 0} s \cdot \{\Gamma_X(s)\}, \\ \gamma_{Y,m} &= \lim_{s \rightarrow 0} s \cdot \{\Gamma_Y(s)\}.\end{aligned}\quad (34)$$

Using the symmetry conditions along with Eq. (9), the limits evaluate to

$$\begin{aligned}\gamma_{X,m} &= \gamma_m \cdot \frac{[k_{M_x, \gamma_X}(\infty) + k_{s\gamma}] \cdot k_{s\gamma}}{[k_{M_x, \gamma_X}(\infty) + k_{s\gamma}]^2 + k_{M_y, \gamma_X}(\infty)^2}, \\ \gamma_{Y,m} &= \gamma_m \cdot \frac{-k_{M_y, \gamma_X}(\infty) \cdot k_{s\gamma}}{[k_{M_x, \gamma_X}(\infty) + k_{s\gamma}]^2 + k_{M_y, \gamma_X}(\infty)^2}.\end{aligned}\quad (35)$$

From this equation, the total steady state response is found by vector addition,

$$\tilde{\gamma}_{s,m} = \gamma_{X,m} \tilde{e}_X + \gamma_{Y,m} \tilde{e}_Y, \quad (36)$$

where the constant amplitude of $\gamma_{s,m}$ is

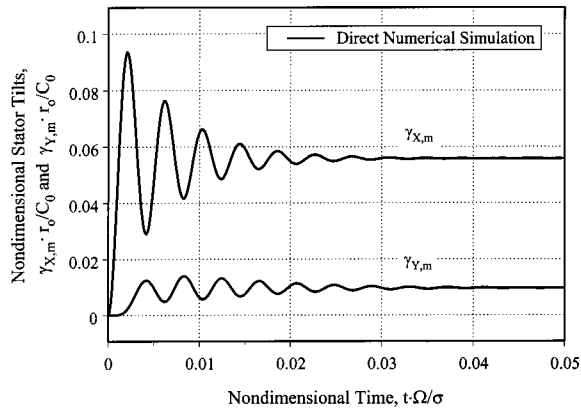


Fig. 7 X and Y components of stator tilt response to initial stator misalignment alone computed by numerical simulation ($\Omega = 2094.4$ rad/s)

$$\gamma_{s,m} = \gamma_m \cdot \frac{k_s \gamma}{\sqrt{[k_{M_X} \cdot \gamma_X(\infty) + k_s \gamma]^2 + k_{M_Y} \cdot \gamma_X(\infty)^2}} \quad (37)$$

This is a static response and, therefore, does not contain inertia terms.

For comparison, a numerical simulation of motion for an initial stator misalignment of $\gamma_m \cdot r_o / C_0 = 5.0$ is given in Fig. 7. From the data in the figure, the steady-state tilt amplitudes are $\gamma_{X,m} \cdot r_o / C_0 = 5.58(10)^{-2}$ and $\gamma_{Y,m} \cdot r_o / C_0 = 9.66(10)^{-3}$. These values yield a total response amplitude of $\gamma_{s,m} \cdot r_o / C_0 = 5.66(10)^{-2}$. Now, using the closed-form expression in Eqs. (35) and (37) with the constitutive model parameters found in Table 2, values of $\gamma_{X,m} \cdot r_o / C_0 = 5.56(10)^{-2}$, $\gamma_{Y,m} \cdot r_o / C_0 = 9.63(10)^{-3}$ and $\gamma_{s,m} \cdot r_o / C_0 = 5.64(10)^{-2}$ are computed. The differences in the nonlinear numerical solution and the correspondence principle results are all within 0.4 percent.

Steady-State Response to Both Rotor Runout and Initial Stator Misalignment. For the situation when both rotor runout and static stator misalignment are present, the principle of superposition is employed to find the total steady-state response. Adding $\tilde{\gamma}_{s,r}$ from Eqs. (32) and $\tilde{\gamma}_{s,m}$ from Eqs. (35) and (36) yields the total stator response,

$$\tilde{\gamma}_s = [\gamma_r A \cos(\Omega t - \phi) + \gamma_{X,m}] \tilde{e}_X + [\gamma_r A \sin(\Omega t - \phi) + \gamma_{Y,m}] \tilde{e}_Y \quad (38)$$

This vector addition is illustrated in Fig. 8: the total stator response vector is a sum of $\tilde{\gamma}_{s,r}$, which precesses about Z at a speed Ω , and $\tilde{\gamma}_{s,m}$, which is stationary in the inertial XY frame. The amplitude of the stator response is

$$\gamma_s^2 = \gamma_{s,r}^2 + \gamma_{s,m}^2 + 2\gamma_{s,r}[\gamma_{X,m} \cos(\Omega t - \phi) + \gamma_{Y,m} \sin(\Omega t - \phi)], \quad (39)$$

and it precesses at a rate of $\psi = \Omega$. For this case, $\gamma_{X,m}$ is much greater than $\gamma_{Y,m}$ so that $\gamma_{s,m} \approx \gamma_{X,m}$ is a valid approximation. Simplifying Eq. (39) then yields

$$\gamma_s^2 \approx \gamma_{s,r}^2 + \gamma_{s,m}^2 + 2\gamma_{s,r}\gamma_{s,m} \cos(\Omega t - \phi). \quad (40)$$

When $\Omega t - \phi = n\pi$, where n is an integer, then γ_s takes on maximum and minimum values of $\gamma_s = |\gamma_{s,r} \pm \gamma_{s,m}|$. When plotting γ_s from Eq. (40), the result is a pure sinusoid oscillating about a constant offset. The amplitude of the constant offset, or average value of the response, is the maximum of $\gamma_{s,r}$ and $\gamma_{s,m}$, and the amplitude of the superimposed oscillation is the minimum of $\gamma_{s,r}$ and $\gamma_{s,m}$. An example of the stator response computed by numerical simulation is plotted in Fig. 9 for the case when $\gamma_m \cdot r_o / C_0 = 5.0$ and $\gamma_r \cdot r_o / C_0 = 2.0$, which correspond to the values from the separate analyses previously discussed. As depicted in the fig-

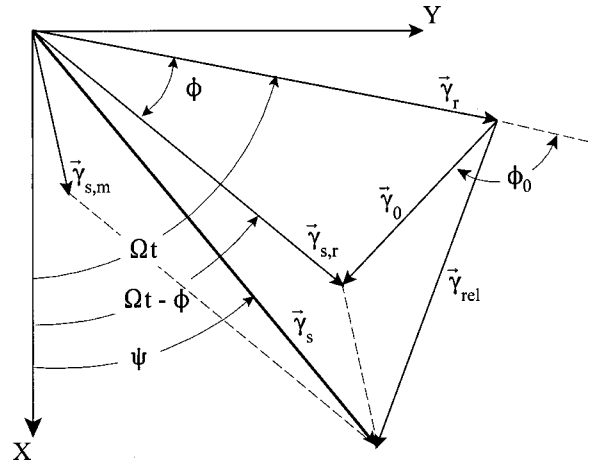


Fig. 8 Tilt vector diagram showing the relationship among the stator tilt responses

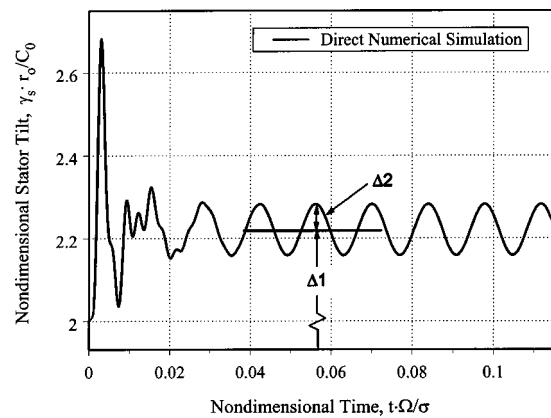


Fig. 9 Stator tilt response to rotor runout and initial stator misalignment computed by numerical simulation ($\Omega = 2094.4$ rad/s)

ure, the average value of the total response at steady-state is $\Delta 1 = 2.22$, and the oscillation amplitude is $\Delta 2 = 6.18(10)^{-2}$.

For the correspondence principle, the responses to rotor runout and initial stator misalignment are computed separately and then combined for the total response. Recall previously that the correspondence principle predicted steady-state responses of $\gamma_{s,m} \cdot r_o / C_0 = 5.66(10)^{-2}$ and $\gamma_{s,r} \cdot r_o / C_0 = 2.22$ when the misalignments were studied separately. In this instance, the constant offset would equal $\gamma_{s,r}$, and the oscillation amplitude would be $\gamma_{s,m}$. The correspondence principle and the numerical simulation give identical results for $\Delta 1$, whereas the values for $\Delta 2$ differ by 8.4 percent.

For the seal studied here, the nonlinear numerical simulation predicts a non-zero steady-state axial response to such a large rotor runout ($\gamma_r \cdot r_o / C_0 = 2.0$). However, the amplitude of this response is small compared to the large rotor runout and corresponding stator response amplitudes. The linearized analysis by the correspondence principle could not predict such behavior since the axial mode and angular modes are completely decoupled in the analysis.

Transmissibility

In seal analysis, designers use transmissibilities as important indicators of the seal dynamic tracking ability. For instance, the

transmissibility $|\gamma_{s,r}/\gamma_r|$ represents the ratio of the steady-state amplitude of the stator response to rotor runout amplitude. From Eq. (33),

$$\left| \frac{\gamma_{s,r}}{\gamma_r} \right| = A, \quad (41)$$

where A is given in Eqs. (30). A very large or very small value for $|\gamma_{s,r}/\gamma_r|$ indicates that the stator is not tracking the rotor well. A ratio close to unity is preferred. For the seal studied earlier, the transmissibility is $|\gamma_{s,r}/\gamma_r| = 1.105$, which indicates good tracking behavior. Another important performance indicator is the ratio of stator response at steady-state to static stator misalignment, $|\gamma_{s,m}/\gamma_m|$. From Eq. (37), this ratio is

$$\left| \frac{\gamma_{s,m}}{\gamma_m} \right| = \frac{k_{s\gamma}}{\sqrt{[k_{M_X, \gamma_X}(\infty) + k_{s\gamma}]^2 + k_{M_Y, \gamma_X}(\infty)^2}}. \quad (42)$$

Small values for $|\gamma_{s,m}/\gamma_r|$ are preferred to facilitate better tracking between the stator and rotor. From the example presented earlier, $|\gamma_{s,m}/\gamma_r| = 0.0113$, which is relatively small.

These two transmissibility ratios do not give information regarding the phase difference between the stator and rotor tilt vectors. Even if the rotor and stator tilt amplitudes were similar, a large phase difference between them can lead to excessive leakage or face contact. The better tracking indicator is the transmissibility relating the ratio of the relative tilt vector to the runout amplitude. The relative tilt vector at steady-state can be written from Eq. (2) as

$$\tilde{\gamma}_{rel} = \tilde{\gamma}_{s,m} + \tilde{\gamma}_0, \quad (43)$$

where

$$\tilde{\gamma}_0 = \tilde{\gamma}_{s,r} - \tilde{\gamma}_r. \quad (44)$$

Here, $\tilde{\gamma}_0$ is the relative misalignment when $\gamma_m = 0$ (see Fig. 8). Utilizing the definition of $\tilde{\gamma}_r$ in Eq. (1) along with Eq. (32), $\tilde{\gamma}_0$ can be written in complex notation as

$$\tilde{\gamma}_0 = A_0 \gamma_r e^{j(\Omega t - \phi_0)}, \quad (45)$$

where A_0 is a complex number defined as

$$A_0 = A e^{-j\phi} - 1, \quad (46)$$

and where ϕ_0 is found from

$$\tan(\phi_0) = \frac{\sin(\phi)}{A \cos(\phi) - 1}. \quad (47)$$

From this derivation, it is clear that the amplitude of $\tilde{\gamma}_0$ is constant, and it precesses with speed Ω with a lag of ϕ_0 behind the rotating vector, $\tilde{\gamma}_r$. The transmissibility $|\gamma_0/\gamma_r|$ is then found to be

$$\left| \frac{\gamma_0}{\gamma_r} \right| = |A_0| = |A e^{-j\phi} - 1|. \quad (48)$$

Now, to find $|\gamma_{rel}/\gamma_r|$, consider the following inequality from Eq. (43):

$$|\tilde{\gamma}_{rel}| \leq |\tilde{\gamma}_{s,m}| + |\tilde{\gamma}_0|. \quad (49)$$

A maximum limit for $|\gamma_{rel}/\gamma_r|$ is derived by dividing both sides of this equation by γ_r and rearranging, giving

$$\left| \frac{\gamma_{rel}}{\gamma_r} \right|_{max} = \frac{\gamma_m}{\gamma_r} \left| \frac{\gamma_{s,m}}{\gamma_m} \right| + \left| \frac{\gamma_{s,r}}{\gamma_r} \right|. \quad (50)$$

Low values for this transmissibility are ideal and indicate that the seal exhibits superior dynamic tracking ability. Figure 10 shows γ_{rel} from a nonlinear numerical simulation for the seal with $\gamma_m \cdot r_o / C_0 = 5.0$ and $\gamma_r \cdot r_o / C_0 = 2.0$. From the data in the figure, the maximum value of γ_{rel} at steady-state is 0.288, which yields a transmissibility ratio of $|\gamma_{rel}/\gamma_r|_{max} = 0.144$. The correspondence

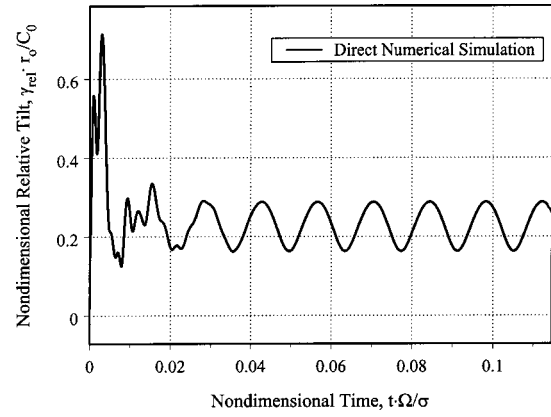


Fig. 10 Relative tilt response to rotor runout and initial stator misalignment computed by numerical simulation ($\Omega = 2094.4$ rad/s)

principle gives $|\gamma_{rel}/\gamma_r|_{max} = 0.135$, which is within 6 percent of the value from the numerical simulation. Since the average amplitude of the relative tilt vector is approximately 0.3, which is relatively large, this prediction by the correspondence principle (based on linearization) is considered a very good approximation.

Stability

Dynamic instability is a significant issue relevant to the practical operation of mechanical face seals. The gas film correspondence principle generates closed-form expressions for the characteristic equations for these seals, from which their stability can be investigated. While the method of stability analysis is general, the following discussion pertains to the particular face seal design with parameters listed in Table 1, gas film properties illustrated in Figs. 3 and 4, and constitutive model parameters in Table 2. Furthermore, since the storage and loss moduli for the axial mode of this seal are strictly positive regardless of shaft speed (see Fig. 4(a)), the coefficients of the characteristic Eq. (22) are also positive. This fulfills the necessary and sufficient conditions for unconditional stability for this mode. Therefore, only instability in the tilt modes will be investigated.

The characteristic equation for the tilt modes is given in Eq. (28). The numerical simulation and the correspondence principle both verify that this seal is stable for the geometry and inertia properties stated in Table 1. However, as the transverse moment of inertia increases, a critical point, I_{crit} , is reached above which the seal is unstable. At this critical point, at least one of the eigenvalues of Eq. (28) has a zero real part, so in theory, the seal will exhibit a sustained whirl at the corresponding frequency, ω_{crit} . To find I_{crit} , the quantity $j\omega_{crit}$ replaces s in Eq. (28), and the resulting frequency equation is separated into real and imaginary parts and solved for ω_{crit} and I_{crit} using an algorithm for nonlinear equations. Note, however, that the product of I_{crit} and ω_{crit}^2 will appear in the resulting equations. This product, $(I \cdot \omega^2)_{crit}$, was found to be the critical indicator of stability threshold in reference [3], and Eq. (28) analytically confirms the same result for the seals studied here. For this problem, values of $\omega_{crit} = 1788.0$ rad/s and $I_{crit} = 0.0229$ kg·m² were computed. Note at stability threshold, ω_{crit} is significantly higher than half the shaft speed ($\Omega = 2094.4$ rad/s). This behavior is inherent to the spiral groove geometry (see [11]). To verify these results, the misalignments were set to zero and the transient responses were computed by nonlinear numerical simulation for values of I above, equal to, and below I_{crit} . The stator mass and moment of inertia were assumed to be related by $I = 1/2 m \cdot r_o^2$, so the mass corresponding to I_{crit} is $m_{crit} = 12.74$ kg. The three stator responses are shown in Fig. 11. The response envelopes for two of these cases (I

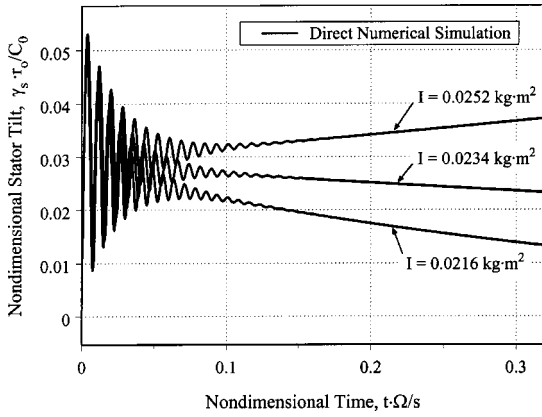


Fig. 11 Stator tilt response to initial velocity conditions near stability threshold computed by numerical simulation ($\Omega = 2094.4$ rad/s)

$= 0.0216 \text{ kg} \cdot \text{m}^2$ and $I = 0.0234 \text{ kg} \cdot \text{m}^2$) decay gradually, indicating they are stable. The response for $I = 0.0252 \text{ kg} \cdot \text{m}^2$ continues to grow, indicating it is unstable at the presumed equilibrium point. Therefore, the critical moment of inertia predicted by the full nonlinear numerical simulation is between $I = 0.0234 \text{ kg} \cdot \text{m}^2$ and $I = 0.0252 \text{ kg} \cdot \text{m}^2$. Although the correspondence principle under-predicts I_{crit} , the difference is relatively small. To pinpoint the exact value for I_{crit} using numerical techniques is an arduous procedure (see discussion by Green and Barnsby [3]), but this value can be predicted fairly precisely in closed-form using the correspondence principle (within 8 percent, in this example).

It is emphasized that the characteristic equation is found in closed-form in terms of the inertia, support and gas film properties. Therefore, it is ideal for parametric study especially for cases where the parameters being varied do not influence the gas film properties. Examples of such parameters include the inertial properties and the support properties. In these cases, once the constitutive model has been obtained, the stability threshold can be found very quickly for various ranges of the parameters directly from the characteristic equation without computationally intensive numerical solution.

Conclusions

A constitutive model is given for representing the stiffness and damping properties of thin gas films in mechanical face seals. The constitutive model is found by curve fitting the step responses or frequency responses with a cosine-modified Prony series. The series conveniently stores the time and frequency domain properties using only a few constants. This work also employs the gas film correspondence principle for the semi-analytical dynamic analysis of gas lubricated face seals. The correspondence principle is derived from the gas film constitutive law, which governs the relationship among the generalized gas film forces, seal motion, and the step responses. The validity of the constitutive law and correspondence principle is predicated upon the assumption that the generalized gas film forces behave linearly with respect to motion, which is approximately satisfied if the motion remains small about equilibrium. This linearized method, however, would also provide quality insight about trends in the problem even if large excursions from equilibrium were considered.

Several analytical solutions are made available by the gas film correspondence principle. Closed-form solutions are found for the natural response to initial velocity conditions. Also, expressions are given for the characteristic equations, from which are computed critical inertia values that yield seal instability. The steady-state responses to rotor runout and initial stator misalignment are derived, and closed-form expressions are given for the transmissibility ratios of the stator responses to the misalignment ampli-

tudes. The most critical transmissibility ratio for indicating tracking performance is the relative tilt transmissibility, $|\gamma_{\text{rel}}/\gamma_r|$, because it measures both the relative amplitude and phase difference between the seal rings. Each of these analytical solutions from the correspondence principle compare well with direct numerical simulations that include nonlinear effects. The superb agreement between the linear and nonlinear analysis techniques indicates that no significant nonlinear effects were revealed by the nonlinear simulation and that the constitutive model accurately represents the gas film properties.

This semi-analytical dynamic analysis technique has the potential for saving a significant amount of time in the design of mechanical face seals. Often during the design process, many cases are considered before a final design is chosen. It is this situation where the semi-analytical technique offers the most significant advantage. As long as the gas film parameters remain the same, the stiffness and damping properties only need to be computed once, after which the constitutive model acts as a kernel of solution for the Reynolds equation. In this case, a design can be investigated in closed-form to find the effect of a change in any system parameter, such as mass, support stiffness, etc., with relative ease and quickness. The semi-analytical technique can also be used to give approximate solutions if the changes are small in the system parameters that affect the gas film properties.

Acknowledgment

This work was supported in part by an NSF Graduate Research Traineeship through Grant No. EEC-9256289 while the first author was at the Georgia Institute of Technology. This support is gratefully acknowledged.

Nomenclature

- $a_{11}, a_{12}, a_{21}, a_{22}$ = matrix coefficients from tilt equation of motion
- A = amplitude of stator response to rotor runout
- A_0 = amplitude of relative misalignment vector when $\gamma_m = 0$
- $A_{i,j,n}$ = amplitude coefficient for constitutive model
- b_1, b_2 = matrix coefficients from tilt equation of motion
- C = clearance between centerlines of rotor and stator
- C_0 = design clearance between rotor and stator at equilibrium
- $d_{s,Z}, d_{s,\gamma}$ = axial and tilt damping of stator support
- $D_{i,j}$ = gas film damping
- \vec{e}_X, \vec{e}_Y = unit vectors in X and Y directions
- \vec{e}_θ = unit vector in θ direction
- F_Z = gas film axial force
- $F_{Z,\text{eq}}$ = gas film axial force at equilibrium
- f_i = generalized force
- $f_{i,\text{eq}}$ = generalized force at equilibrium
- $G_{i,j}$ = gas film frequency response
- $G_{i,j}^*$ = nondimensional frequency response; axial, $G^* = G \cdot C_0 / (P_a r_o^2)$; tilt, $G^* = G \cdot C_0 / (P_a r_o^4)$
- \bar{G} = frequency response matrix
- h = film thickness separating stator and rotor
- I = stator transverse moment of inertia
- I_{crit} = stator transverse moment of inertia at stability threshold
- Im = imaginary part
- j = imaginary number, $\sqrt{-1}$
- $k_{i,j}$ = gas film step response
- $k_{i,j}^*$ = nondimensional step response; axial, $k^* = k \cdot C_0 / (P_a r_o^2)$; tilt, $k^* = k \cdot C_0 / (P_a r_o^4)$
- $k_{s,Z}, k_{s,\gamma}$ = axial and tilt stiffness of stator support

$K_{i,j}$ = Laplace or Fourier transform of $k_{i,j}$
 \bar{k} = step response matrix
 m = Stator mass
 m_{crit} = Stator mass at stability threshold
 M_X, M_Y = gas film moments about X and Y -axes
 M_{Xi} = moment from initial stator misalignment
 N_g = number of grooves
 P_a = ambient pressure
 p = gas pressure
 p_i, p_o = gas pressure at inner and outer radial boundaries
 r = radius, radial coordinate
 Re = real part
 r_i, r_o, r_j = inner, outer and sealing dam radii
 s = Laplace variable
 $S_{i,j}$ = gas film stiffness
 t = time
 w_g, w_l = width of groove and land regions
 XYZ = inertial reference frame
 x_j = generalized coordinate or degree of freedom
 Z = axial displacement of stator from equilibrium clearance
 $\alpha_{i,j,n}$ = exponential decay coefficient for constitutive model
 α_g = spiral groove angle
 β = groove width fraction
 δ_g = groove depth
 γ_m = amplitude of initial stator misalignment
 γ_X, γ_Y = amplitudes of stator tilts about X and Y -axes
 $\gamma_{X,m}, \gamma_{Y,m}$ = amplitudes of steady-state stator tilts about X and Y -axes for response to initial stator misalignment
 $\gamma_0, \vec{\gamma}_0$ = relative misalignment amplitude and vector when $\gamma_m=0$
 $\gamma_r, \vec{\gamma}_r$ = rotor runout amplitude and vector
 $\vec{\gamma}_{\text{rel}}$ = relative tilt vector between stator and rotor
 $\gamma_s, \vec{\gamma}_s$ = Stator tilt amplitude and vector
 $\gamma_{s,m}, \vec{\gamma}_{s,m}$ = steady-states stator tilt amplitude and vector for response to initial stator misalignment alone
 $\gamma_{s,r}, \vec{\gamma}_{s,r}$ = steady-state stator tilt amplitude and vector for response to rotor runout alone
 Γ_X, Γ_Y = Laplace transforms of γ_X and γ_Y
 Λ = compressibility number, $6\mu\Omega r_o^2/(P_a C_0^2)$
 μ = gas viscosity
 $\nu_{i,j,n}$ = oscillation frequency coefficient for constitutive model

σ = squeeze Number, $12\mu\Omega r_o^2/(P_a C_0^2)$
 ϕ = phase difference between stator response and rotor runout
 ϕ_0 = phase difference between relative misalignment and rotor when $\gamma_m=0$
 $\phi_{i,j,n}$ = frequency shift coefficient for constitutive model
 ω = excitation frequency
 ω_{crit} = whirl frequency at stability threshold
 Ω = shaft rotational speed

Subscripts

i = corresponding to the generalized force: F_Z , M_X , or M_Y
 j = corresponding to the generalized displacement: Z , γ_X , or γ_Y

References

- [1] Shapiro, W., and Colsher, R., 1974, "Steady State and Dynamic Analysis of a Jet-Engine, Gas Lubricated Shaft Seal," *ASLE Trans.*, **17**, pp. 190–200.
- [2] Leefe, S., 1994, "Modeling of Plain Face Gas Seal Dynamics," *14th Int. Conf. Fluid Sealing, BHR Group Conference Series No. 9*, B. Halligan, ed., Professional Engineering Publishing, Suffolk, UK, pp. 397–424.
- [3] Green, I., and Barnsby, R. M., 2001, "A Simultaneous Numerical Solution for the Lubrication and Dynamic Stability of Noncontacting Gas Face Seals," *ASME J. Tribol.*, **123**(2), pp. 388–394.
- [4] Miller, B., and Green, I., 2001, "Numerical Formulation for the Dynamic Analysis of Spiral-Grooved Gas Face Seals," *ASME J. Tribol.*, **123**(2), pp. 395–403.
- [5] Ruan, B., 2002, "Numerical Modeling of Dynamic Sealing Behaviors of Spiral Groove Gas Face Seals," *ASME J. Tribol.*, **124**(1), pp. 186–195.
- [6] Green, I., and Barnsby, M. R., 2002, "A Parametric Analysis of the Transient Forced Response of Noncontacting Gas Coned Face Seals," *ASME J. Tribol.*, **124**(1), pp. 151–157.
- [7] Green, I., and Etsion, I., 1985, "Stability Threshold and Steady-State Response of Noncontacting Coned-Face Seals," *ASLE Trans.*, **28**, pp. 449–460.
- [8] Malanoski, S. B., and Pan, C. H. T., 1965, "The Static and Dynamic Characteristics of the Spiral-Grooved Thrust Bearing," *ASME J. Basic Eng.*, **87**, pp. 547–558.
- [9] Zirkelback, N., and San Andrés, L., 1999, "Effect of Frequency Excitation on Force Coefficients of Spiral Groove Gas Seals," *ASME J. Tribol.*, **121**(4), pp. 853–863.
- [10] Ruan, B., 2002, "A Semi-Analytical Solution to the Dynamic Tracking of Non-Contacting Gas Face Seals," *ASME J. Tribol.*, **124**(1), pp. 196–202.
- [11] Miller, B., and Green, I., 2002, "Numerical Techniques for Computing Rotor-dynamic Properties of Mechanical Gas Face Seals," *ASME J. Tribol.*, **124**(4), pp. 755–761.
- [12] Gross, W. A., 1980, *Fluid Film Lubrication*, John Wiley & Sons, New York.
- [13] Miller, B., and Green, I., 1998, "Constitutive Equations and the Correspondence Principle for the Dynamics of Gas Lubricated Triboelements," *ASME J. Tribol.*, **120**(2), pp. 345–352.
- [14] Elrod, H. G., Jr., McCabe, J. T., and Chu, T. Y., 1967, "Determination of Gas-Bearing Stability by Response to a Step-Jump," *ASME J. Lubr. Technol.*, **89**, pp. 493–498.
- [15] Miller, B., and Green, I., 1997, "On the Stability of Gas Lubricated Triboelements Using the Step Jump Method," *ASME J. Tribol.*, **119**(1), pp. 193–199.